ISSN (Print) 1226-1750
ISSN (Online) 2233-6656
Journal of Magnetics 25(3), 355-362 (2020) https://doi.org/10.4283/JMAG.2020.25.3.355

Design Optimization of Brush Permanent Magnet DC Motors Using Response Surface Method

Youn-Hwan Kim[1,2], Do-Hyeop Kim[1], Jae-Won Moon[1], and Sang-Young Jung[2]*

[1]*Rotating Machinery Center, Korea Testing Certification, Gunpo 15809, Republic of Korea*
[2]*Department of Electrical and Computer Engineering, Sungkyunkwan University, Suwon 16419, Republic of Korea*

(Received 9 April 2020, Received in final form 15 September 2020, Accepted 17 September 2020)

This paper describes design modifications and optimization of a brush permanent magnet DC motor. The test model was optimized using the analytical method via an equivalent circuit, and the final model simulation was performed using the finite element method (FEM). For the optimization method, a central composite design of the response surface analysis was used, and torque and current ripples were analyzed using 2-D FEM. The back-to-back test method was used to evaluate the developed model to minimize the burden on the construction of the test equipment. The test results were validated through a comparison of the analysis results.

Keywords : back-to-back test, brush permanent magnet DC motor, central composite design, optimization, response surface analysis

1. Introduction

Brushed DC motors are widely used in applications ranging from toys to adjustable car seats, cooling fans, and sunroof motors for automobiles. The speed of brushed DC motors can be varied by changing the operating voltage or the strength of the magnetic field. The largest merit of brushed DC motor is the low price. Therefore, it is still not replaceable in certain areas. Brushed motors were the first commercially important application of electric power to drive mechanical energy, and DC distribution systems were used for more than 100 years to operate motors in commercial and industrial buildings. They have a long history, but still have requirements for further research.

The armatures of brushed DC motors are generally associated with stator poles fabricated from low-cost ceramic ferrite magnets with magnetic flux densities of approximately 0.4 T [1]. Magnets are often longer than the laminated rotor core to provide an axial flux concentration effect.

Research on vibration mitigation is rare. There are two types of vibration modes, pulsating force and bending moment. The relationships between these two vibrations and pole width, pole number, and slot number are analyzed for vibration mitigation [2, 3].

The finite element method (FEM) is one of the most valuable tools in electric machine design as it accurately considers nonlinear materials and complex geometries [4]. However, the design procedure is based on trial and error which is time-consuming and uncertain. This is the primary drawback and can be eliminated by combining FEM with an analytical method by equivalent circuit and response surface method (RSM). The exact modeling of the leakage flux in an electrical machine is seemingly impossible using the analytical method, which is verified using FEM [5].

Response surface analysis predicts outcomes for any variable in the region of interest. This is a statistical analysis method that optimizes the variables to obtain the desired result. The response values that change according to the different variables can be represented as two or three-dimensional surfaces, making them visually identifiable. RSM is still a popular methodology in the optimization of electrical machines [6-9].

This paper presents a design methodology for cylindrical brush DC permanent magnet motors. This methodology is primarily based on analytical models employing RSM optimization process to determine the best machine characteristics that maximize the torque and minimize the current of the brushed DC motor. The final developed

*Corresponding author: Tel: +82-31-299-4952
Fax: +82-31-290-7231, e-mail: syjung@skku.edu

model was validated using FEM and a back-to-back test [10].

2. Design Methodology

2.1. Analytical method using an equivalent circuit

The structure of a PM brush DC motor is shown in Fig. 1.

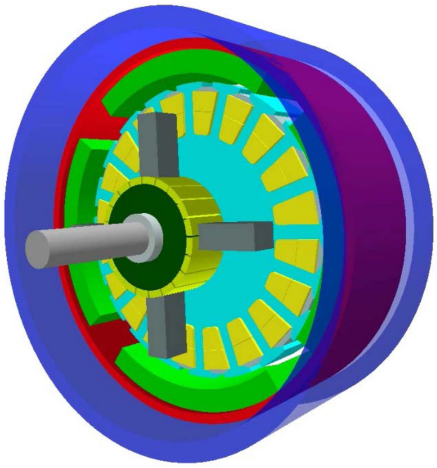

Fig. 1. (Color online) Structure of PM brush DC motor.

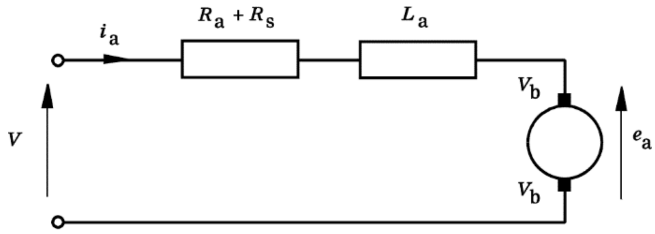

Fig. 2. Electric circuit model of PM brush DC motor.

1 and the electric circuit model in Fig. 2 [11]. V is the terminal voltage, i_a is the instantaneous armature current, e_a is the instantaneous back-EMF, V_b is the volt-drop in each brush, R_a is the armature resistance, R_s is the resistance of the supply including leads, and L_a is the armature inductance. The mathematical model is represented by (1)

$$V = e_a + (R_a + R_b)i_a + L_a\frac{di_a}{dt} + 2V_b \tag{1}$$

The armature resistance R_a is calculated from the winding details. Assuming that the supply leads have no resistance, the armature resistance is expressed as (2).

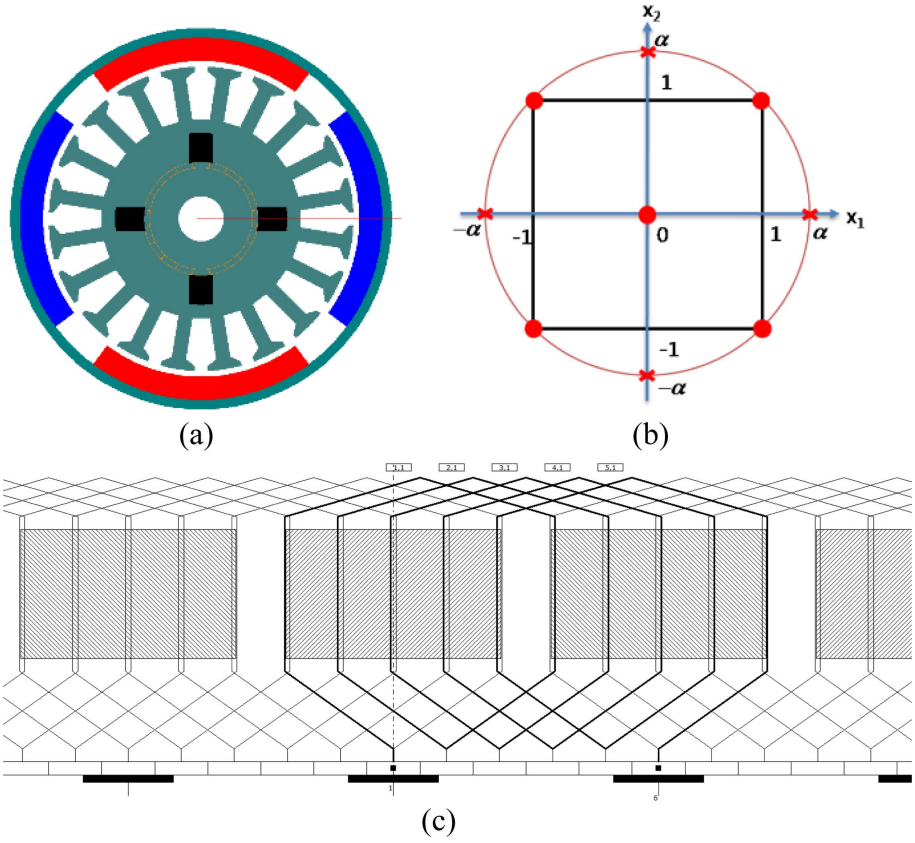

Fig. 3. (Color online) Design for PM brush DC motor. (a) Cross section of the example. (b) Central composite design of RSM. (c) Coil in lap-wound DC armature.

$$R_a = \rho_{cu} \times \frac{Z \times MLT/2a^2}{NSH \times \pi d_{cu}^2/4} \quad (2)$$

where NSH is the number of strands-in-hand in each conductor, d_{Cu} is the strand diameter, ρ_{cu} is the resistivity of copper, MLT is the mean length of turn, a is the number of parallel paths, and Z is the total number of armature conductors.

The armature inductance L_a is also calculated from the winding details and motor geometry. This calculation is considerably more complex than that of the resistance, and the theory is provided in detail in [12]. e_a is obtained from the magnetic circuit model as in (3) and (4).

$$e_a = k_e \omega_m \quad (3)$$

$$k_e = \frac{PZ\Phi_g}{a\pi} \quad (4)$$

The flux/pole Φ_g is calculated in the magnetic circuit model. ω_m is the angular velocity in rad/sec, equal to $2\pi \times$ RPM/60. Figure 1 shows the electric circuit model of a PM brush DC motor, and Fig. 3 shows the design cross section, central composite design, and coil in lap-wound DC armature of the PM brush DC motor.

Full-pitch coils are mostly used in DC machines [13]. The lap winding is suitable for high-current and low-voltage DC because there are many parallel circuits, and the wave winding is suitable for high-voltage and low-current because of two parallel circuits. In consideration of this theory, the coil span was designed to be 5 with lap winding.

Table 1. Parameters of the PM brush DC motor.

Quantity	Value	Unit
Rated power	150	W
Rated speed	1850	r/min
Poles	4	-
Slot	20	-
Stack length of rotor	15	mm
Stator outer radius	50	mm
Rotor outer radius	39.9	mm
Height of PM	23	mm
Coercive force of PM	–250,000	A/m

Table 2. The objective function and the range of design variable.

Objective Function	Torque	Maximize
	Current	Minimize
Range of design variable	$126 \le \text{BetaM} \le 166$	
	$3.0 \le L_M \le 7.0$	
	$3.2 \le B_{width} \le 7.2$	
	$-10 \le B_{shift} \le 30$	

2.2. Response surface analysis

The response surface analysis is largely performed in three stages.

1) Screening test: Select key factors among the factors that are considered to affect the response.

2) Response surface analysis: Perform experiments using the central composite design or the Box-Behnken design method under optimal conditions, and explore the

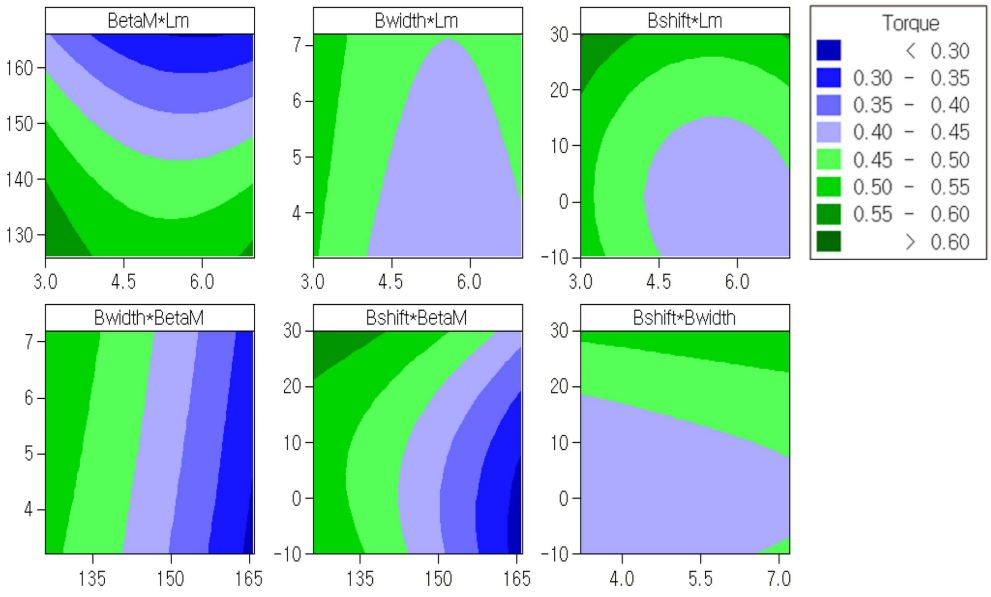

Fig. 4. (Color online) Contour plots of torque by changing of design variables.

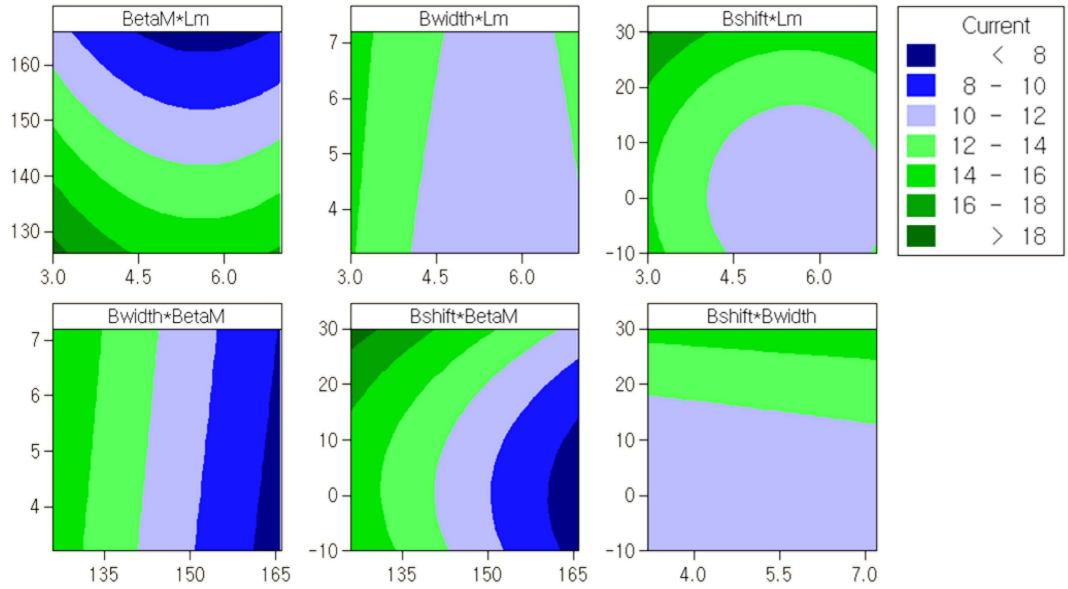

Fig. 5. (Color online) Contour plots of current by changing of design variables.

optimal conditions of the variables that optimize the response values in the region of interest.

3) Confirmation of reproducibility: Check the significance of the model created in the response surface analysis, and compare the expected response value with the actual experimental result after performing the actual experiment under optimized conditions.

Box-Behnken designs often have fewer design points than central composite designs, thus, they are less expensive to operate with the same number of factors. However, Box-Behnken designs always have three levels per factor, unlike central composite designs that can have up to five [14]. A central composite design is the most commonly designed experiment in the response methodology; hence, it is used for the optimization of the PM brush DC motor. Table 2 lists the objective function and range of design variables. *BetaM*, L_M, B_{width} and B_{shift} are the length of the permanent magnet, thickness of the permanent magnet, thickness of brush, and installation angle of the brush. Figure 4 and Fig. 5 shows the contour plots of torque and current as design variables change.

Figure 6 shows the results of the response optimization. The adjusted coefficients of multiple determinations R^2_{adj} which indicate the reliability of the model are 99.5 % and 99.9 % for torque and current, respectively.

2.3. 2-D finite element method

As the next step, simulating the optimized model using FEM solution seems necessary for the confirmation of reproducibility. FEM is a numerical method for solving engineering problems, and transient simulation is essential for the final validation of performances before the realization of the prototype. The FEM solution generally requires boundary value problems for partial differential equations. The 2-D governing equation of the electromagnetic analysis field domain is expressed as (5).

$$\nabla \times \left(\frac{1}{\mu}\nabla \times \vec{A}\right) + \sigma\left(\frac{\partial \vec{A}}{\partial t} + \nabla\phi\right)\vec{J}_s \tag{5}$$

where μ is the magnetic permeability, $\vec{A}$ is the magnetic vector potential, σ is the conductivity, ϕ is the magnetic flux, and $\vec{J}_s$ is source current density,

Figure 7 shows the results of the FEM analysis which are the magnetic flux density, torque ripple, and current ripple. The magnetic flux density was the largest in the stator near the permanent magnets, and the rotor magnetic flux density was relatively small. The average torque, torque ripple, average current and current ripple were

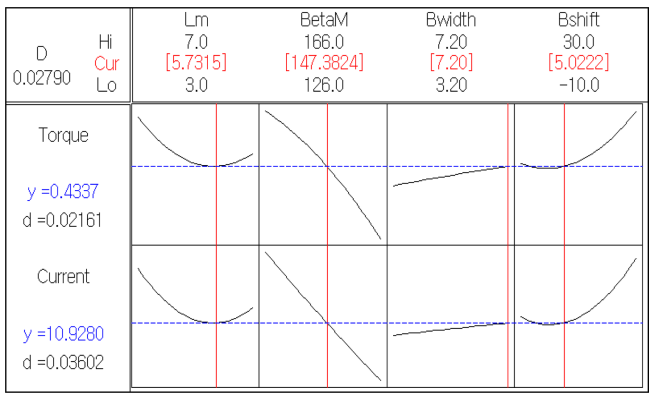

Fig. 6. (Color online) Result of response optimization.

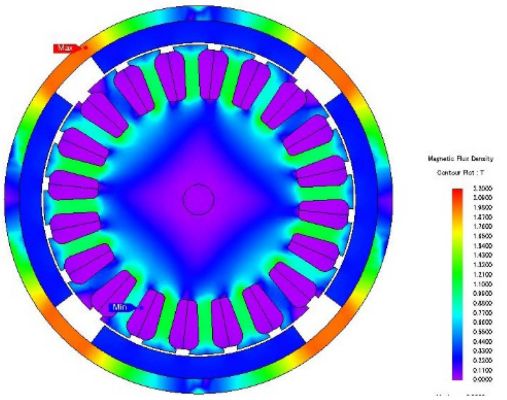

(a)

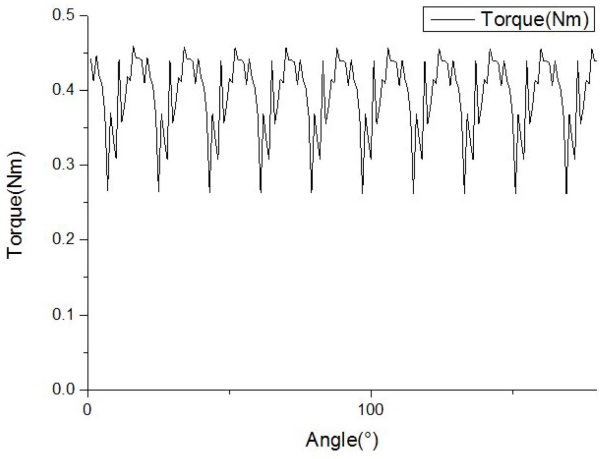

(b)

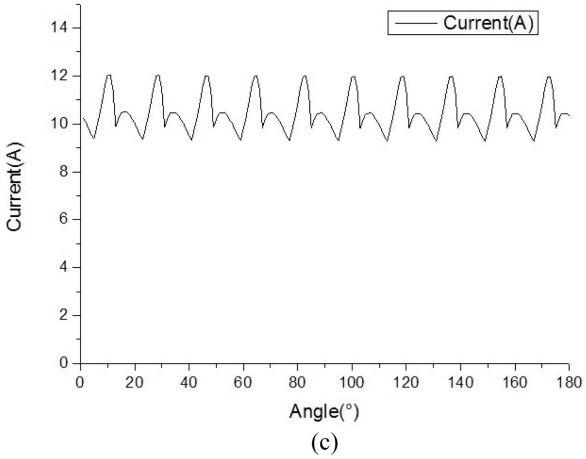

(c)

Fig. 7. (Color online) Result of 2D FEM analysis (a) Magnetic flux density (b) Torque ripple (c) Current ripple.

calculated as 0.46 Nm, 41 %, 10.8 A, 26 %, respectively.

3. Test and Verification

3.1. DC motor back-to-back test

The back-to-back test is a simple efficiency test performed by connecting two identical motors. The current delivered from the power source generates a magnetic field through the rotor of the drive motor. At that moment, the current flowing through the winding generates a copper loss in the drive motor. The copper loss of a motor is simply a product of its winding resistance and current. For the driving motor to generate a torque through the air gap, magnetic flux is generated in the laminated core, and in this process, iron losses such as hysteresis and eddy current losses occurs. Because the value of iron loss changes according to the frequency of the rotor field, the driving motor and the generating motor connected through the rotating shaft is assumed to have the same value.

Instead of using a mechanical measurement method utilizing torque and speed, which are relatively difficult to measure, the efficiency of the motor can be estimated by measuring the electrical input and output using two motors with the same characteristics. After separating the copper losses from the driving motor and generating motor, the efficiency is calculated using (6), assuming

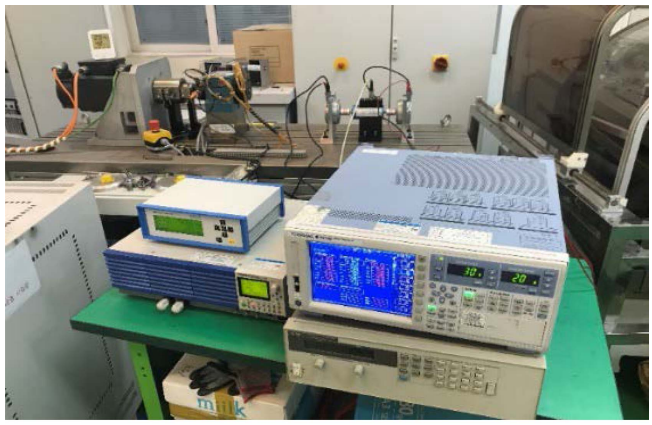

(a)

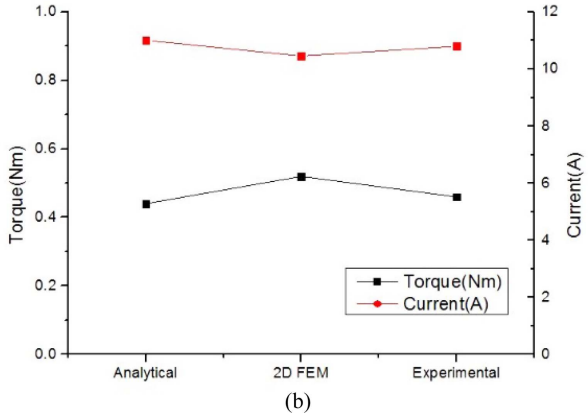

(b)

Fig. 8. (Color online) (a) DC motor back-to-back test setup (b) Comparison of DC motor simulation and test.

that the same amount of iron and mechanical losses exist in both motors. Finally, the torque is estimated as (7).

$$\eta = \frac{1}{2} + \frac{P_{g,out} - L_{m,copper} + L_{g,cooper}}{2P_{in}} \tag{6}$$

$$Torque = \frac{P_{in} \times \eta \times 60}{RPM \times 2\pi} \tag{7}$$

Figure 8 shows the comparison of the simulation and the test results of the DC motor. The torque result of 2D FEM was 0.52 Nm, which was higher because no mechanical and wind losses were reflected. The simulation results of DC motor current were compared with the of the experiment, and were within a 5 % deviation.

3.2. Measurement uncertainty analysis

The efficiency measurement is a critical issue in the market of motors that concerns electric motor manufacturers, suppliers, consumers, and market surveillance authorities. Generally, due to the instrumentation used, instability phenomena internal to the object under testing, and effects produced by external phenomena, the repetition of a measurement process provides a set of data that are close to each other, but not identical [15]. The evaluation of uncertainty by internationally recognized GUM [16] guidelines is carried out in accordance with the procedure as shown in the Fig. 9.

The measurement uncertainty is specified by the variance of the measurable value of the variable related to the measurement result. The measurement uncertainty is specified by the variance of the measurable value of the variable related to the measurement result. That is, the output variable Y is expressed by the estimated output y and the measurement uncertainty U as (8).

$$Y = y \pm U \tag{8}$$

The uncertainty component is classified into type A evaluation, which is a method of evaluation of uncertainty by the statistical analysis of series of observations, and type B evaluation, which is a method of evaluation of uncertainty by means other than the statistical analysis of series of observations. In order to reduce the uncertainty of type A evaluation, it is necessary to obtain enough raw measured data through repeated tests about torque, rotational speed, voltage, current and resistance. Type B evaluation is obtained using previous measurement data, experience with or related to the behavior and properties of relevant materials and instruments, manufacturer's specifications, data provided in calibration and other certificates. The combined standard uncertainty of the measurement results is denoted by $u_c(y)$ and represents the estimated standard deviation of the measured object.

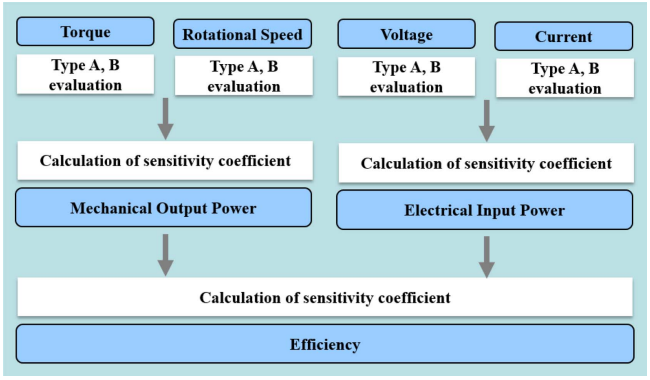

Fig. 9. (Color online) Flowchart of uncertainty evaluation about the motor efficiency.

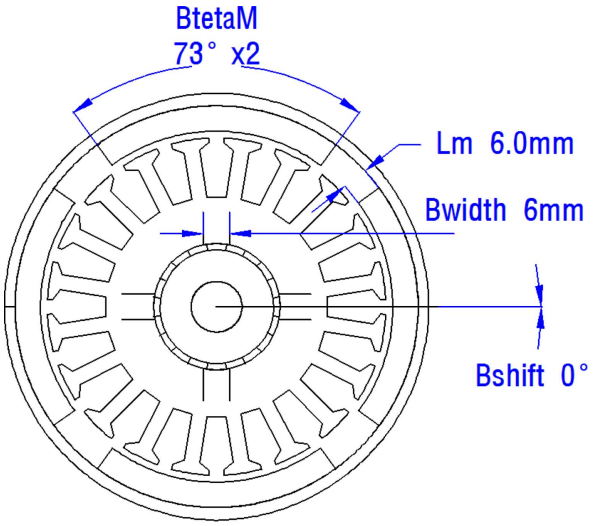

(a)

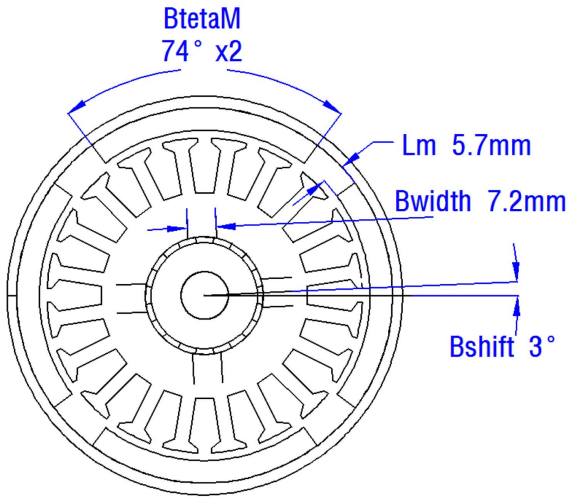

(b)

Fig. 10. (a) The initial model (b) The optimized model.

In general, the combination of standard uncertainties is obtained by propagation of uncertainty. The method of estimating the combined standard uncertainty is divided into the case where there is no correlation, as in (9):

$$u_c(y) = \sqrt{\sum_{i=1}^{n} \left(\frac{\partial f}{\partial x_i}\right)^2 u^2(x_i)} \tag{9}$$

The direct efficiency determination requires the direct measurement of motor output power P_2 and input power P_1:

$$\eta_d = \frac{P_2}{P_1} \tag{10}$$

Whose uncertainty is

$$u_c(\eta_d) = \sqrt{\left(\frac{1}{P_1}\right)^2 \cdot u(P_2)^2 + \left(-\frac{P_2}{P_1^2}\right)^2 \cdot u(P_1)^2} \tag{11}$$

Motor output power P_2 is calculated by using the measured torque M and speed n values from torque meter and tachometer.

$$P_2 = \frac{2\pi \cdot n \cdot N}{60} \tag{12}$$

$$u_c(P_2) = \sqrt{\left(\frac{2\pi \cdot n}{60}\right)^2 \cdot u(N)^2 + \left(\frac{2\pi \cdot n}{60}\right)^2 \cdot u(n)^2} \tag{13}$$

$u(N)$ and $u(n)$ is standard uncertainties for torque and speed. They are derived using (9), which combines A-type and B-type evaluation. The expanded uncertainties are obtained by using the coverage factor that transformed the combined standard uncertainty into a 95 % confidence interval. The value of the coverage factor k is usually between 2 and 3. In this study, k = 2 is used in consideration of the effective degrees of freedom.

The overall measurement results for the determination of the measurement uncertainty are summarized in Table 3 and Table 4. Finally, the efficiency based on the test was 60.1 % ± 0.8 %, and the efficiency of the optimal model was within the uncertainty range.

Table 3. Central Values and Standard Uncertainties.

Measured quantities	Central Value	Standard Uncertainty
Rotating Speed	1857 r/min	0.3 r/min
Torque	0.44 Nm	0.003 Nm
Phase current	10.83 A	0.01 A
Input Power	142.41 W	0.24 W

Table 4. Instrument Standard Uncertainties.

Measuring Instrument	Range	Standard Uncertainty
Voltmeters	100 V	0.01 V
Ammeters (CT)	50 A	0.01 A
Wattmeters	240 W	0.02 W
Torque meters	2 Nm	0.002 Nm
Tachometer	10000 rpm	0.5 rpm

4. Conclusion

In this paper, the design optimization of a brush permanent magnet DC motor was investigated. The length of the permanent magnet, thickness of permanent magnet, thickness of brush and installation angle of brush were used as design variables for optimization. Figure 10 shows the initial and optimized model of the DC motor. The torque increased from 0.435 Nm to 0.437 Nm and the current decreased from 11.120 A to 11.095 A. As a result, the efficiency increased and the results were verified using back-to-back test.

Acknowledgments

The authors acknowledge the support provided by the Korea Technology and Information Promotion Agency (TIPA) and funding by the Ministry of SMEs and start-ups of Korea. The research project no. is S2857726.

References

[1] J. Cros, G. C. R. Sincero, and P. Viarouge, IEEE Trans. Ind. Applicat **26**, 786 (1990).
[2] S. Wang, J. Hong, Y. Sun, J. Shen, H. Cao, and Z. Yang, IEEE Trans. Energy Convers. **33**, 1411 (2018).
[3] J. Hong, S. Wang, Y. Sun, and H. Cao, IEEE Trans. Indust. Electr. **66**, 3595 (2019).
[4] L. Jolly, M. A. Jabbar, and L. Qinghua, IEEE Trans. Magn. **41**, 3928 (2005).
[5] R. Tarvirdilu-Asl, R. Zeinali, and H. B. Ertan, Proc. 2017 Intl Aegean Conference on Electrical Machines and Power Electronics (ACEMP), May, 2017, 401 (2017).
[6] K. Y. Hwang, S. B. Rhee, B.Y. Yang, and B. I. Kwon, IEEE Trans. Magn. **43**, 1833 (2007).
[7] D. K. Hong, J. H. Choi, D. J. Kim, Y. D. Chun, B. C. Woo, and D. H. Koo, IEEE Trans. Magn. **49**, 4088 (2013).
[8] T. Ishikawa, M. Yamada, and N. Kurita, IEEE Trans. Magn. **47**, 1290 (2011).
[9] H. S. Shin, K. H. Shin, T. K. Bang, G. H. Jang, and J. Y. Choi, Proc. KIEE, 71 (2018).
[10] S. H. Won, Trans. KIEE, **63**, 143 (2014).

[11] User's Manual, CD-adapco, PC-DCM 3.9, Aug. (2011).
[12] T. J. E. Miller, M. I. McGilp, D. A. Staton, and J. J. Bremner, Proc. IEE Eelctr. Pow. Appilct 129 (1999).
[13] P. C. Sen, Principles of Eletric. Machines and Powr. Electronics, 3rd ed., Wiley, 141 (2015).
[14] X. K. Gao, F. T. S. Low, Z. J. Liu, and S. X. Chen, IEEE Trans. on Magn. **38**, 1141 (2002).
[15] G. Bucci, F. Ciancetta, E. Fiorucci, S, Mari, and M. A. Segreto, Energies **13**, 78 (2020).
[16] ISO/IEC GUIDE 98-3:2008 Uncertainty of Measurement Part 3.